Advancing Pile-Bearing Capacity Prediction With Meta-Heuristic Enhanced Specific ANFIS Strategys

Zhongmiao Dang*

Zhengzhou Vocational College of Finance and Taxation; Zhengzhou Henan, 450000, China

Corresponding author. E-mail: 18239967193@163.com

Received: Sep. 19, 2024; Accepted: Feb. 09, 2025

In the wake of demands for efficiency, this investigation offers a novel strategy for the real-time prediction of PBC. This method is developed using specific ANFIS predictive schemes, sturdinessened by two robust meta-heuristic schemes: ARO and CryStal. The integration of these schemes enhances the accuracy of the prediction while simplifying the process. The following study presents three schemes: the ANCS, the ANAR, and the individual ANFIS strategy. Each model adds different aspects to the whole, synergistically enhancing overall precision in PBC prediction. This strategy signifies a radical improvement in PBC prediction strategies by introducing an effective and time-saving method with extensive geomechanical applications. Meta-heuristic schemes combined with specific ANFIS schemes show promising outcomes toward real-time PBC estimation in diverse geological scenarios. Notably, the statistical performance of the ANCS model is very impressive with an R^2 value of 0.999 for the whole database in a validation test and with a minimum RMSE of 49.24. Moreover, the ANCS model has displayed very good predictive and generalization performance compared to developed ANFIS and ANAR schemes, hence emphasizing its efficiency and applicability for real-world problems.

Keywords: Pile Bearing Capacity (PBC); Adaptive neuro-fuzzy inference system; Artificial Rabbits Optimization; Crystal Structure Algorithm.

http://dx.doi.org/10.6180/jase.202512_28(12).0004

1. Introduction

Because of the intricate and diverse traits of soil behavior and its evolving interplay with structural components, the appraisal of *PBC* arises as a significant challenge within the domain of geotechnics [1, 2]. Over the years, reputable academics have suggested some methodologies to forecast *PBC*. Some methodologies, including pile static and empirical investigation, call for including essential safety factors through some simplifications. Conversely, other strategies, such as pile loading tests, while renowned for their reliability, they often entail substantial setup expenses and time investments. The cone penetration test (*CPT*) is among the most commonly employed in-situ testing strategies in the industry [3]. The various advantages of *CPT* are that it is rapid to execute, simple, and comparatively inexpensive. Because of the inherent similarities to the structural components in question, this test is most commonly used to estimate PBC. Smooth data at discrete soil depths is available with this. Specifically, the cone tip of the penetrometer resembles the tip of the pile and the cone sleeve mimics the friction surface of the pile for precise estimations. There are two strategies commonly adopted when using *CPT* outcomes for pile design [4]. One is the indirect approach whereby PBC is determined from soil properties interpreted from *CPT* outcomes, while the second, which can be referred to as a direct strategy, determines *PBC* directly from *CPT* data [5]. In the direct strategy domain, it has become a widely accepted practice to use computational intelligence for predicting *PBC* based

on *CPT* findings. Even though there has been a tremendous amount of development in geotechnical engineering and soil mechanics, the task of figuring out *PBC* is still complex. The complicated interaction between piles complicates the representation of these situations along with the constantly changing properties of the soil and the variety of pile characteristics. Elements such as soil anisotropy, moisture content, and complex stress-strain patterns increase the intricacy of the duty [6, 7]. Additionally, local differences can affect pile traits such as substance composition, pile type, construction strategies, shape, and installation strategies [8].

The investigation of analytical and semi-experimental strategies, though valuable, may result in less accurate projects of *PBC* as a result [9, 10]. A growing number of researchers have recommended integrating artificial intelligence (*AI*) methodologies due to the high expenses linked to conventional laboratory and field tests for deep foundations and the urgent need to optimize pile design [11, 12]. These Machine Learning (*ML*) schemes have become a powerful and flexible solution that provides additional and alternative strategies to established strategies for estimating *PBC* [13]. Furthermore, to ensure the dependability of the predictions produced by these sophisticated schemes, meticulous preprocessing, feature engineering, and thorough model verification are crucial steps [3, 14–16].

Some visionary investigators have recommended the utilization of AI strategies, considering the high costs of laboratory and field tests for deep foundations and the urgent need for pile design optimization. In geotechnical engineering, ML schemes have now become an important tool and a promising alternative to traditional strategies [17, 18]. These schemes carefully simulate the complex interactions between soil and piles using pattern recognition and large databases, ultimately increasing the accuracy of *PBC* predictions [19].

Gu et al. [20] sought to enhance PBC , a critical factor that arises during pile foundation design. This work introduced a new methodology based on CBO combined with a multi-layer perceptron neural network and ANFIS. The outcomes showed high accuracy by CBO-MLP and CBO-ANFIS schemes: the R^2 values are 0.9874 (training), 0.9785 (validation), and 0.987 (test). The comparative analysis showed that these schemes performed better than traditional strategies and, therefore, were more reliable and efficient in the estimation of PBC in pile foundation design. Chen [21] sought the highly accurate prediction of PBC using Random Forest schemes with the improvement of two meta-heuristic schemes, Snake Optimizer and Equilibrium Optimizer. In this investigation, three schemes (RFEO, RFSO, and a single RF model) were developed and evaluated on a database of PBC samples coming from various types of soil obtained through the stabilization test. The input variables selected are Average Cohesion, Average Friction Angle, Average Soil Specific Weight, Average Pile-Soil Friction Angle, Flap Number, Pile Area, and Pile Length. The outcomes revealed that the RFSO scheme was the best among the developed schemes with an R^2 of 0.998 and the lowest RMSE of 109.43, showing consistency in better generalization and prediction capability. It presented an effective, thus time-saving methodology that enabled the estimation of real-time PBC with important applications in geomechanics, especially in various geological scenarios. Kardani et al. [22] investigated six ML schemes, namely DT, KNN, MLP, RF, support vector regressor, and XGBoost, for estimating PBC in cohesionless soil. The schemes were trained using PSO for hyperparameter tuning on a database of 59 cases and evaluated on R^2, RMSE, and VAF. The optimized XGBoost model performed the best, $R^2 = 0.9615$, while effective stress had the highest importance score, 30.9%. Comparisons with the β-method show that optimized ML schemes outperform their counterparts in terms of accuracy, demonstrating the potential for geotechnical applications.

While these studies indicate the development of PBC predictive modeling, most of them are based on single optimization strategies or traditional machine learning schemes, which may suffer from slow convergence, local optima problems, and the inability to adapt to different geotechnical conditions. Further, the development of schemes that integrate advanced optimization schemes with the ANFIS scheme for enhancing prediction accuracy and computational efficiency is still highly desired. This paper tries to fill these gaps by introducing a new strategy that combines ANFIS with two state-of-the-art meta-heuristic schemes, namely ARO and the Crystal Structure Algorithm (CryStal). Contrary to previously developed strategies, this research shows that the integration of such schemes will overcome the limitations regarding exploration-exploitation trade-offs and yields superior predictive performance in a wide range of geological scenarios.

The reason for the selection of ARO and CryStal is their better performance to overcome the challenges of PBC predictions. Both schemes have efficient convergence and are very capable in escaping local minima; hence, they are quite apt for the non-linear, multi-modal solution landscapes common in PBC problems. ARO balances global and local searches effectively, hence its adaptability to different databases; the structure-inspired mechanism of CryStal ensures its robustness in high-dimensional search domains.

Recent studies showed that these schemes outperform conventional schemes like PSO and GA in terms of accuracy, convergence speed, and computational efficiency. Their adaptive search mechanisms and robustness in handling the complexity of constraints are suitable for the variability and nonlinear nature of geotechnical data sets. ARO and CryStal integration with ANFIS represents a new strategy that develops the complementary sturdinesss of the schemes involved and thus assures improved accuracy with wider applicability for real-time geotechnical applications. This is an innovative combination compared to the strategies previously in use, thus justifying the adoption of ARO and CryStal in this investigation.

2. Materials and methodology

2.1. Data gathering

An indepth review of PBC in the context of soil would involve the consideration of many factors in great detail [12]. To optimize efficiency, the database was separated into three subsets: training (70%), validation (15%), and testing (15%). This research analysis relies on a database of 231 experimental samples from prior investigations. This database validates the empirical distribution method and sturdinessens predictive schemes [11, 23]. The input variables contains seven following variables, which the statistical properties presents in Table 1.

- Average Cohesion: It represents the soil's cohesive sturdiness, a critical factor influencing pile behavior.
- Average Friction Angle: It governs its shear sturdiness and impedance to sliding along planes.
- Average Soil Specific Weight: The specific weight of the soil impacts its compactness and, consequently, its load-bearing property.
- Average Pile-Soil Friction Angle: This angle characterizes the pile and surrounding soil interaction, impacting the load transfer mechanism.
- Flap Number: The count of flaps or protrusions on the pile's surface can influence its interaction with the soil and, thus, its PBC.
- Pile Area: The cross-sectional area of the pile significantly contributes to its loadbearing capacity by determining the contact domain with the soil.
- Pile Length: It is pivotal in identifying its penetration depth into load-bearing strata, consequently affecting its total property.

The primary objective of collecting this data is to set an in-depth and representative database for training and examining predictive schemes, ultimately leading to accurate PBC estimation [24]. Fig. 1 visually illustrates the frequency spread of each variable via a cumulative histogram plot.

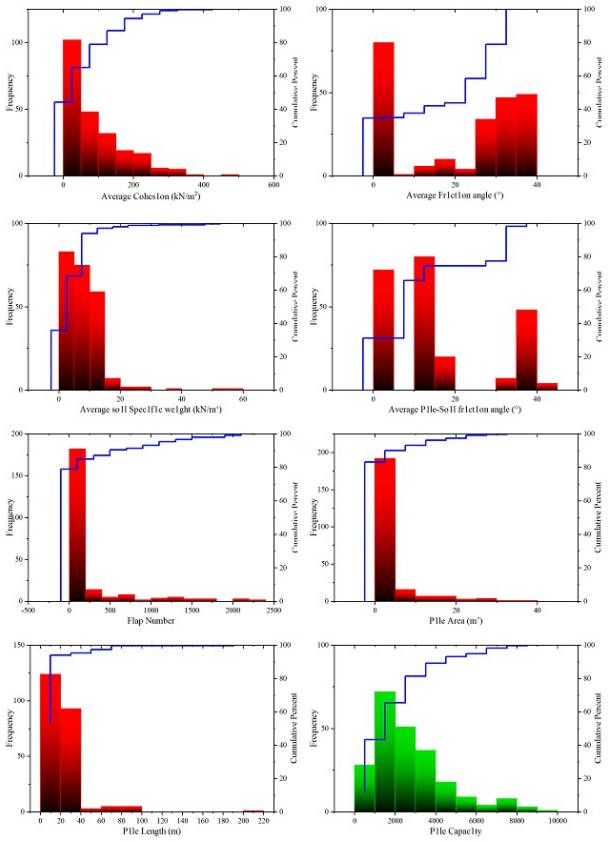

Fig. 1. The visualization of the cumulative histogram between the input and output.

2.2. ANFIS

$ANFIS$ demonstrates significant potential for tackling function approximation issues using neural networks [25]. To set a relational mapping between input and output, $ANFIS$ is employed. Fuzzy logic (FL) and ANN) are employed in $ANFIS$. This investigation recommends a scheme that fosters an $ANFIS$ modeling scheme that is more systematic, diminishing the trust in expertise. The $ANFIS$ architecture comprises several nodes with diverse node functions throughout all layers [26]. The nodes of the layer above act as the present layer's input. The preseent discourse presumes that a system utilizing two inputs (x, y) and one output (f_i) is considered for simplicity and clarity to express the strategies employed by $ANFIS$. In the scheme of

Table 1. The statistic traits of the input of PBC.

Factors	Indicators				
	Category	Min	Max	Avg	St.Dev.
Average Cohesion $(\mathrm{kN/m^2})$	Input	0.00	475.00	93.08	83.66
Average Friction angle $(^\circ)$	Input	0.00	39.00	19.97	15.35
Average soil Specific weight $(\mathrm{kN/m^2})$	Input	0.00	55.51	7.23	7.71
Average Pile - Soil friction angle $(^\circ)$	Input	0.00	41.00	15.21	13.77
Flap Number	Input	0.00	2291.00	214.28	464.36
Pile Area $(\mathrm{m^2})$	Input	0.01	35.72	3.10	6.25
Pile Length (m)	Input	3.00	207.00	22.57	19.10
Pile Capacity (KN)	Output	480.00	9350.00	2723.35	1836.33

a first-order Sugeno fuzzy inference system, the two rules may be stated as:

Rule 1:If x is E_1 and y is D_1 then c is $f_1(x, y)$

Rule 2: If x is E_2 and y is D_2 then c is $f_2(x, y)$

Functions A and B, which display the outcomes of a Sugeno fuzzy inference system of the first order, are employed by $ANFIS$ to inputs x and y. Fig. 2 displays the $ANFIS$ configuration, with each layer encompassing the node functions outlined below. The circles display constant nodes with factors that do not alter in the system; in contrast, the squares symbolize flexible nodes that allow metric collections to be modified [27].

- *Layer*1: The flexible functions of the nodes in this layer are as follows:

$$O_{1,i} - \mu_{E_i}(X) \text{ for } i = 1, 2 \tag{1}$$

$$O_{1,i} - \mu_{D_i}(y) \text{ for } i = 3, 4 \tag{2}$$

E and D display the linguistic labels, while x and y represent the input nodes. The highest and lowest values of the membership functions $\mu(x)$ and $\mu(y)$, often shaped like bells, are 1 and 0 , respectively. This can be stated as:

$$\mu(x) = \frac{1}{1 + \left(\frac{x - s_i}{e_i}\right)^{2d_i}} \tag{3}$$

$$\text{Or} \quad \mu(x) = \exp\left\{-\left(\frac{x - s_i}{e_i}\right)^2\right\} \tag{4}$$

The set of factors e_i, d_i, and s_i are employed, with the corresponding parameter values adjusting the bell-shaped functions, which serve as variables. These variables, often referred to as premise factors, establish the structure of the functions.

- *Layer*2: Every node acts as a constant point, indicated with the name Π and displayed by a circle. The function of these nodes is to multiply the input signals and create the relevant output signals.

$$O_{2,i} = \vartheta_i = \mu_{E_i}(X) \cdot \mu_{D_i}(y) \quad \text{for } i = 1, 2 \tag{5}$$

The degree of activation of a rule is depicted by the output variable ϑ_i.

- *Layer*3: A circle and the letter M are used to identify each node as a constant node within this certain layer. The node's duty is to standardize its firing sturdiness by measuring the ratio between the firing sturdiness of the ith node and the total firing sturdinesss of all rules.

$$O_{3,i} = \varphi_i = \frac{\vartheta_i}{\sum \vartheta_i} = \frac{\vartheta_i}{\vartheta_1 + \vartheta_2} \quad \text{for } i = 1, 2 \tag{6}$$

- *Layer*4: Each node is recognized by a square, has a flexible nature, and performs a certain node function.

$$O_{4,i} = \varphi_i . f_i \quad \text{for } i = 1, 2 \tag{7}$$

The fuzzy set of if-then rules is displayed by f_1 and f_2 in the way in which:

Rule 1: If x is E_1 and y is D_1 then $f_1 = q_1 x + p_1 y + z_1$

Rule 2: If x is E_2 and y is D_2 then $f_2 = q_2 x + p_2 y + z_2$

The factors set, namely q_i, p_i, and z_i, are named after the ensuing factors.

- *Layer*5: Each node is stationary, performing a node function that measures the total output.

$$O_{5,i} = f_{\text{out}} = \sum_i \varphi_i . f_i = \text{ overall output} \tag{8}$$

The total output can be stated as a linear aggregation of the resulting factors utilizing the ANFIS strategy previously discussed [28]. Consequently, the final result can be illustrated as follows:

$$\begin{aligned} sf_{\text{out}} = \varphi_1 f_1 + \varphi_2 f_2 = \frac{\vartheta_1}{\vartheta_1 + \vartheta_2} f_1 + \frac{\vartheta_2}{\vartheta_1 + \vartheta_2} f_2 = \\ (\varphi_1 x)\, q_1 + (\varphi_1 y)\, p_1 + (\varphi_1)\, z_1 + \\ (\varphi_2 x)\, q_2 + (\varphi_2 y)\, p_2 + (\varphi_2)\, z_2 \end{aligned} \tag{9}$$

The derivatives of the squared error associated with each node output are dispatched as error signals during the backward pass from the output layer to the input layer. In this pass, the gradient descent scheme adjusts the premise factors.

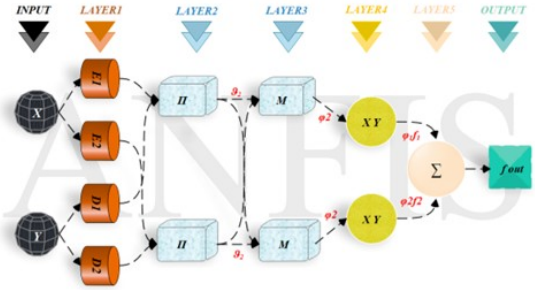

Fig. 2. ANFIS architecture.

2.3. ARO

ARO was influenced by the survival tactics employed by rabbits in their natural habitat. The detour foraging strategy, where rabbits venture away from their nests to seek food, served as the basis for this strategy [17]. Fig. 3 illustrates the process of *ARO* [29].

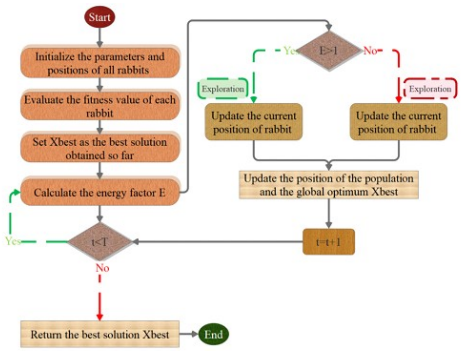

Fig. 3. The process of *ARO*.

2.3.1. Energy Shrink (Switch between Exploration and Exploitation)

Rabbits can engage in random hiding or detour foraging, contingent on their energy levels. An energy factor $A(t)$ is computed using Eq. (10) to simulate the rabbit's decision. If $A(t)$ surpasses 1 , the rabbit will opt for detour foraging, whereas if $A(t)$ is less than or equal to 1 , it will choose random hiding.

$$A(t) = 4\left(1 - \frac{t}{T}\right)\ln\frac{1}{r} \tag{10}$$

Here, r displays a haphazardly selected number between 0 and 1 .

2.3.2. Detour Foraging (Exploration)

As per Eq. (11), rabbits haphazardly search for food drawing on the situations of their peers while searching for food away from their nests to shield themselves from potential predators.

$$\begin{aligned}\overrightarrow{S_l}(t+1) &= \overrightarrow{x_j}(t) + U \times \left(\overrightarrow{x_l}(t) - \overrightarrow{x_j}(t)\right) \\ &+ \text{round}\,(0.5 \times (0.05) + r_1)) \times n_1, i, j \\ &= 1, \ldots, n \text{ and } j \neq i\end{aligned} \tag{11}$$

$$U = O \times C \tag{12}$$

$$O = \left(e - e^{\left(\frac{t-1}{T}\right)}\right) \times \sin(2\pi r_2) \tag{13}$$

$$C(k) = \begin{cases} 1 \text{ if } k = g(0) \\ 0 \text{ else} \end{cases} \quad k = 1, \ldots, d \text{ and } l = 1, \ldots, [r_3, d] \tag{14}$$

$$g = \text{randperm}(d) \tag{15}$$

$$n_1 \sim N(0,1) \tag{16}$$

At time t, $\overrightarrow{x_l}(t)$ displays the situation of the ith rabbit, while $\overrightarrow{S_l}(t+1)$ represents the candidate's situation at $t+1$. The maximum count of cycles is T, and the movement pace of rabbits is displayed by L. The rabbit population magnitude is displayed by n , and d represents the count of variables in the problem that requires optimization. Additionally, $r1, r2$, and $r3$ are three random numbers between $(0,1)$, and $n1$ adheres the standard normal distribution. The mapping vector is c, and the running operator that simulates the rabbits' running characteristics is displayed by R.

2.3.3. Random Hiding (Exploitation)

Eq. (17) produces a set of d burrows surrounding the nest of each rabbit. The rabbit haphazardly chooses these burrows for shelter and to avoid potential predators.

$$\overrightarrow{b_{l,j}}(t) = \overrightarrow{x_l}(t) + H \times g \times \overrightarrow{x_l}(t), i = 1, \ldots, n \text{ and } j = 1, \ldots, d \tag{17}$$

$$H = \frac{T - t + 1}{T} \times r_4 \tag{18}$$

$$g(k) = \begin{cases} 1 \text{ if } k = j \\ 0 \text{ else} \end{cases} \quad k = 1, \ldots, d \tag{19}$$

$$\overrightarrow{S_l}(t+1) = \overrightarrow{x_j}(t) + U \times \left(r_4 \times \overrightarrow{b_{l,r}}(t) - \overrightarrow{x_l}(t)\right) i = 1, \ldots, n \tag{20}$$

$$\mathrm{gr}(k) = \begin{cases} 1 \text{ if } k = |r_5 \times d| & k = 1, \ldots, d \\ 0 \text{ else} \end{cases} \tag{21}$$

$$\overrightarrow{b_{l,r}}(t) = \overrightarrow{x_l}(t) + H \times gr \times \overrightarrow{x_l}(t), i = 1, \ldots, n \tag{22}$$

$$\overrightarrow{x_l}(t+1) = \begin{cases} \overrightarrow{x_l}(t) f\left(\overrightarrow{x_l}(t)\right) \leq f\left(\overrightarrow{s_l}(t+1)\right) \\ \overrightarrow{s_l}(t+1) f\left(\overrightarrow{x_l}(t)\right) > f\left(\overrightarrow{s_l}(t+1)\right) \end{cases} \quad k = 1, \ldots, d \tag{23}$$

Eq. (22) highlights $\overrightarrow{b_{l,r}}(t)$ as the haphazardly selected burrow for the *ith* rabbit to take shelter in, where H represents the hiding parameter, $\overrightarrow{b_{l,j}}$ displays the j th burrow for the ith rabbit, and $r4$, and $r5$ display random numbers between $(0, 1)$.

2.4. CryStAl

This article uses the Bravais model to explain the crystal structure [30]. This scheme considers infinite lattice geometry and provides the periodic structure that the lattice geometry defines in the following way, along with the vector of the lattice situations:

$$z = \sum s_i c_i \tag{24}$$

Where c_i symbolizes the primary crystal directions' minimal vector, s_i indicates the crystal's angular number. Modifications appropriate for the mathematical modeling of CryStAl are made to this basic idea of crystals. In this paradigm, every possible enhancement strategy resolution is considered a single crystal lattice. For the cycle's startup, any number of crystal lattices is selected. This paradigm views all potential solutions to optimization strategies as a single crystal lattice. Any number of crystal lattices is selected for the cycle's startup.

$$\begin{bmatrix} wz_1 \\ cwz_2 \\ \vdots \\ wz_i \\ \vdots \\ wz_s \end{bmatrix} = \begin{bmatrix} x_1^1 \ldots & x_1^j \ldots & x_1^q \\ x_2^1 \ldots & x_2^2 \ldots & x_2^q \\ \vdots & \vdots & \vdots \\ x_i^1 \ldots & x_i^2 \ldots & x_i^q \\ \vdots & \vdots & \vdots \\ x_s^1 \ldots & x_s^2 \ldots & x_s^q \end{bmatrix}, \begin{cases} i = 1, 2, 3, \ldots, s \\ j = 1, 2, 3, \ldots, q \end{cases} \tag{25}$$

where q displays the issue's size and s displays the possible resolution. The starting places of these crystals in the search domain are selected at random by:

$$x_i^j(0) = x_{i,\min}^j + \gamma \left(x_{i,\max}^j - x_{i,\min}^j\right), \begin{cases} i = 1, 2, 3, \ldots, s \\ j = 1, 2, 3, \ldots, q \end{cases} \tag{26}$$

Where $x_i^j(0)$ defines the initial gem location, and the lowest and maximum values that are allowed are described as $x_{i,\max}^j$ and $x_{i,\min}^j$ Separately, the i-th candidate arrangement's j - th choice variable falls inside the given ρ. The primary crystals, according to the crystallographic concept of the "*base*", comprise every corner crystal. wz_{main} selected at random while taking into account the initial crystal. In addition, the z_l for every tread, in addition to establishing a random extraction process, the current value is ignored. Crystals whose optimal configuration was established by $wz_r.D_v$ stands for the average of haphazardly selected crystals. Four kinds of revision procedures are developed using fundamental network concepts to monitor the situation of a candidate resolution in the search domain:

Simple cubic;

$$wz_{\text{new}} = wz_{\text{main}} + wz_{\text{old}} \tag{27}$$

Best crystal cubicle;

$$wz_{\text{new}} = z_1 wz_{\text{zmain}} + z_2 wz_r + wz_{\text{old}} \tag{28}$$

Mean crystal cubicle;

$$wz_{\text{new}} = z_1 wz_{\text{zmain}} + z_2 D_v + wz_{\text{old}} \tag{29}$$

M&B crystal cubicle;

$$wz_{\text{new}} = wz_{\text{old}} + z_1 wz_{\text{zmain}} + z_2 wz_r + z_3 D_v \tag{30}$$

In the above formula, the random numbers are displayed by the symbols z, z_1, z_2, and z_3, the new situation is displayed by wz_{new} and the old situation is given by wz_{old} . The two primary parts of metaheuristics are mining and exploration. Notably, tests have been conducted on Eqs. (27) to (30) to ensure that global and local searches may be conducted simultaneously. When variable solutions x_i^j defy the criteria for the variable restrictions, and a mathematical flag is generated that calls for modifying the variable limits, leading to issues with x_i^j surpassing the variable range. The enhancement process terminates when a constant number of cycles is reached, according to the termination criteria [31, 32].

2.5. Execution Appraisal strategies

This investigation employs diverse factors to examine the schemes, including the previously mentioned Performance Index (PI), Correlation Coefficient $\left(\mathrm{R}^2\right), MAE, MAPE$, and $RMSE$. The algorithm's excellent performance during the training, validation, and testing steps is displayed by a high R^2 value. Conversely, lower $RMSE$ and MAE values are preferable because they display less scheme error. Eqs. (31-35) are employed to measure these factors.

- Coefficient of Correlation

$$R^2 = \left(\frac{\sum_{i=1}^{W} (h_i - \bar{h})(q_i - \bar{q})}{\sqrt{\left[\sum_{i=1}^{W} (h_i - h)^2\right]\left[\sum_{i=1}^{W} (q_i - \bar{q})^2\right]}} \right)^2 \quad (31)$$

- Root Mean Square Error

$$RMSE = \sqrt{\frac{1}{W}\sum_{i=1}^{W} (q_i - h_i)^2} \quad (32)$$

- Mean Square Error

$$MSE = \frac{1}{W}\sum_{i=1}^{w} q_i^2 \quad (33)$$

- Mean Absolute Percentage Error

$$MAPE = \frac{100}{W}\sum_{i}^{W} \frac{|q_i|}{|h_i|} \quad (34)$$

- Performance Index

$$PI = \frac{1}{\bar{\bar{q}}} \frac{RMSE}{\sqrt{R^2 + 1}} \quad (35)$$

Here, h_i and q_i display the forecast and experimental values, respectively. The mean values of the experimental samples and expected are displayed by $\bar{h}$ and $\bar{q}$. Alternatively, W displays the count of samples under consideration.

3. Result and discussion

The prediction of PBC values was performed by the ANFIS, ANCS, and ANAR schemes. The schemes were trained by 70%, validated by 15%, tested by 15%, and all data together were used for an overall appraisal (100%). This was done in order to be very fair in the evaluation of their performance. By doing this and applying state-of-the-art methodology, the current study reached more accurate and reliable PBC estimates. This improvement increased the accuracy in the analysis of soils and therefore decision-making in various engineering and construction works. These percentages had been allocated based on the empirical data, which also demonstrated that model performance increased with the same setup. From a further appraisal and algorithm comparison perspective, the work evaluated the five statistical factors of MAPE, MSE, R^2, RMSE, and PI, as detailed in Table 2: A major focus of the appraisal revolved around the R^2 values, which refer to the proportion of the variance in the dependent variable explained by the independent variable. During the validation step, the ANCS model showed the best predictive capability with an excellent R^2 value of 0.999 , outperforming its counterparts.

In contrast, the *ANFIS* model exhibited slightly lower R^2 values during validation, measuring at 0.985 . Beyond R^2 values, the study analyzed additional error indicators, with *RMSE* ranging from 49.24 to 259.83 . It is noteworthy that during validation, the *ANFIS* model displayed the highest *RMSE*, while the *ANCS* model exhibited the lowest. Similarly, the *PI* metric highlighted the *ANFIS* model's peak value of 0.046 during validation, whereas the *ANCS* scheme achieved 0.009 lowest value in the same step. Regarding *MSE*, the *ANFIS* model recorded the highest at 67512.1, while the *ANCS* model emerged as the frontrunner with the most favorable *MSE* values of 2424.5. In terms of *MAPE*, the *ANCS* model demonstrated the lowest and most favorable value of 1.839 during the validation step. Despite the *ANFIS* model showing promise in certain aspects, the comprehensive findings unequivocally established the *ANCS* model's superiority over *ANFIS* and *ANAR* across multiple steps. Ultimately, these outcomes strongly suggest that incorporating CryStal optimization significantly enhanced the *ANFIS* model's ability to anticipate *PBC*, situationing the *ANCS* model as the optimal choice among the evaluated alternatives.

In Fig. 4, a scatter plot is employed to efficiently compare the execution of hybrid schemes based on two key criteria: R^2 and *RMSE*. R^2 assesses the level of agreement, while *RMSE* quantifies the level of spread. The plot is boosted by including a central line and three linear fits showcasing the distinct train, validation, and test steps. All three schemes exhibit remarkable prediction accuracy, showing a robust positive link between the expected and real values. Interestingly, when contrasted with the *ANAR* and ANFIS schemes, the *ANCS* model notably excels in precision. This distinction is particularly evident due to the tight clustering of data points around the central line, reflecting its narrow dispersion range. Conversely, the *ANAR* and *ANFIS* variants exhibit comparable execution levels, with their data points dispersed more broadly.

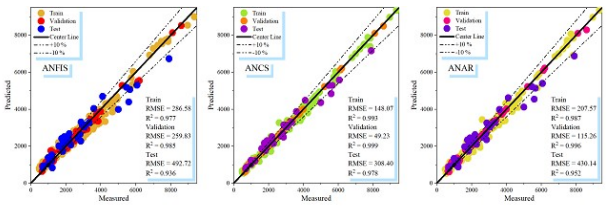

Fig. 4. The hybrid model created a scatter plot.

Fig. 5 presents a comparison between the expected and observed samples. The observed behavior defines the

Table 2. The outcome of ANFIS strategy development.

Model	Phase	Index values				
		RMSE	R^2	MSE	MAPE	PI
ANFIS	Train	286.59	0.978	82131.4	10.926	0.054
	Validation	259.83	0.985	67512.1	8.607	0.046
	Test	492.73	0.937	242782.5	14.609	0.089
	All	321.81	0.973	103562.0	11.117	0.059
ANCS	Train	148.07	0.994	21926.1	4.465	0.028
	Validation	49.24	0.999	2424.5	1.839	0.009
	Test	308.41	0.979	95115.5	8.205	0.055
	All	172.46	0.992	29743.8	4.618	0.032
ANAR	Train	207.57	0.987	43087.1	6.205	0.039
	Validation	115.27	0.997	13286.7	4.648	0.020
	Test	430.15	0.953	185026.6	12.329	0.078
	All	243.85	0.983	59463.4	6.870	0.045

desired state, and the illustration is separated into three segments: training, validation, and testing. In terms of the *ANCS* model, there is a minor discrepancy between the anticipated and observed values, with the testing step generally displaying higher observed values. Likewise, like *ANCS*, the anticipated points for *ANAR* show a slight variance from the observed values, although it is not as precise as *ANCS*. On the other hand, the *ANFIS* scheme showcases a substantial discrepancy and performs less effectively compared to the other two schemes.

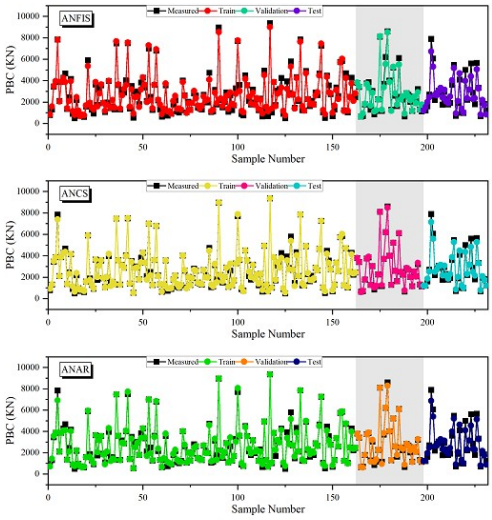

Fig. 5. The comparison of measured and predicted values.

Fig. 6 illustrates a symbol plot crafted to visually represent the error percentages related to the schemes developed in this investigation. This plot effectively captures the unique characteristics of these error distributions. The most noteworthy aspect of the graph is the *ANCS* model, which prominently exhibits the lowest error rate. Most of its error values are concentrated within the 40% range, highlighting the model's impressive accuracy and consistency. Conversely, both the *ANFIS* and *ANAR* schemes display broader error percentage distributions. Their graphs indicate a higher prevalence of values surpassing the 80% and 50% thresholds. Notably, both of these schemes demonstrate a right-skewed spreaed, suggesting the existence of certain data points with significantly elevated error percentages. This visual representation adeptly conveys how error percentages are distributed among the constructed schemes. It effectively emphasizes the exceptional accuracy achieved by the *ANCS* model compared to its counterparts, offering a clear visual depiction of the performance disparities among these schemes.

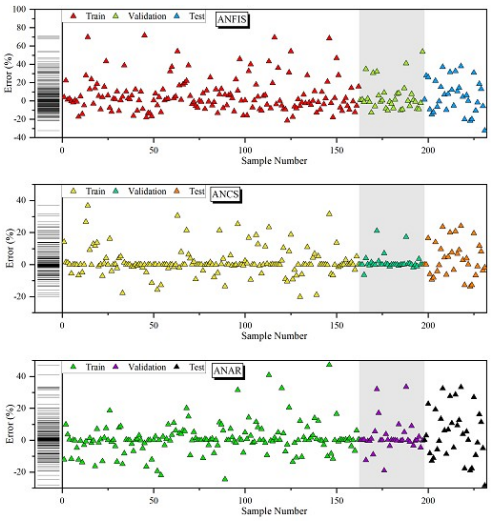

Fig. 6. For hybrid schemes' the error percentage is determined based on the scatter plot.

Fig. 7 compares the three schemes-ANFIS, ANCS, and ANAR-based on their prediction accuracy across training, validation, and testing steps, displayed through the distribution of errors. The primary goal of this figure is to highlight the differences in the schemes' performance, but it presents much information that can be difficult for readers to absorb fully. To make the key insights clearer:

The ANFIS strategy displays significant variability in error distribution, especially during the training step, indicating that the model's predictions are less consistent. The mean error is quite high, which indicates that the model has difficulty in making precise predictions; the large standard deviation shows that its performance may vary depending on the data set. This variability in outcomes could indicate that ANFIS may easily fall into either overfitting or underfitting problems and, hence, may fail to generalize on new, unseen data. In contrast, the error distribution of the ANCS model is a lot narrower in all steps of the prediction, which offers more consistent and reliable estimates. The mean error is near zero, and the spread of errors is compact, showing the accuracy and stability of the model. Smaller standard deviation further recommends the robustness of ANCS and minimal overfitting or underfitting. It leads to a more compact distribution of the error; therefore, the model of ANCS is highly suitable for practical applications since it can generate highly precise forecasts of PBCs on an ensemble of various databases. ANAR gives moderate enhancements over ANFIS, although this model remains behind compared to ANCS. This means that while the ANAR model has better predictions than the ANFIS strategy, it is not as stable as the ANCS model. The mean error is lower than ANFIS, indicating better predictive accuracy, but the more significant standard deviation shows that ANAR is not as consistent in its performance as ANCS.

In the end, the best overall performance is demonstrated by the ANCS model with the lowest mean error and narrow error distribution, reflecting its strong generalization capability and a high degree of reliability. Further, the ANFIS strategy exhibits larger variability and less consistent performance that makes it unsuitable for real-time PBC estimation. While the ANAR model is an improvement over ANFIS, it still does not give the same level of precision and stability as ANCS. Therefore, the use of the ANCS model shall be preferred for accurate, reliable, and real-time PBC prediction for diverse geological scenarios.

4. Conclusion

The pile-bearing capacity (PBC) can be considered one of the most important tasks in geotechnical engineering due to its great impact on construction project security and efficiency. In such a scenario, ML proved to be effective in finding complex patterns for complex databases. Thus, the main goal of the presented investigation was to anticipate PBC employing some advanced ML strategies; the ANFIS strategy was given special emphasis in this respect. This investigation is based on a meticulously selected database with 231 experimental trials and seven input variables from a big collection of published research. Two metaheuristic schemes, ARO and the CryStal, are seamlessly incorporated to enhance the prediction power of the ANFIS strategy. As discussed in the related section, these schemes' predictive power and efficacy in determining PBC features are carefully measured through a thorough analysis of several performance appraisal indicators. This thorough review method produced the above findings.

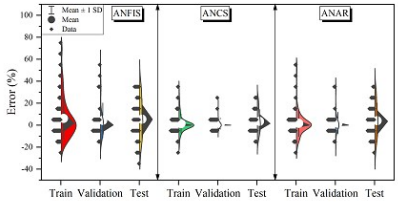

Fig. 7. The violin plot of errors amongst the fostered schemes.

- The outcomes of this investigation show that $ANCS$ schemes perform exceptionally well, producing the highest R^2 values. Even though the $ANFIS$ model shows marginally better values, the difference still exists. Additionally, the $ANCS$ schemes outperform both the $ANFIS$ and $ANAR$ schemes regarding correlation, showing noticeably lower rates, just 1.4%, as opposed to $ANFIS$ than both of those other schemes.
- It is noteworthy that $ANCS$ regularly has the lowest $RMSE$ values across all steps, highlighting its outstanding accuracy and dependability in PBC forecast. It is noteworthy that $ANCS$'s $RMSE$ are significantly 81% lower than those of the baseline $ANFIS$ model.
- It is noteworthy that the MSE values for the ANCS model are 96% lower than those of the standard ANFIS model. This significant decrease highlights the $ANCS$'s noticeably improved predictive performance.
- As a result, the ANCS schemes stand out for their exceptional predictive power, achieving the highest values and the minimal error rates in this investigation, solidifying their situation as the peak performers in estimating PBC.

References

[1] B. T. Pham, T.-A. Hoang, D.-M. Nguyen, and D. T. Bui, (2018) *"Prediction of shear strength of soft soil using machine learning methods"* **Catena *166***: 181–191. DOI: https://doi.org/10.1016/j.catena.2018.04.004.

[2] G. G. Tejani, B. Sadaghat, and S. Kumar, (2023) *"Predict the maximum dry density of soil based on individual and hybrid methods of machine learning"* **Advances in engineering and intelligence systems 2**: 98–109. DOI: 10.22034/aeis.2023.414188.1129.

[3] H. M. Coyle, R. E. Bartoskewitz, and W. J. Berger, (1973) *"Bearing Capacity Prediction by Wave Equation Analysis–state of the Art"*:

[4] I.-M. Lee and J.-H. Lee, (1996) *"Prediction of pile bearing capacity using artificial neural networks"* **Computers and geotechnics *18***: 189–200. DOI: https://doi.org/10.1016/0266-352X(95)00027-8.

[5] W. Chen, P. Sarir, X.-N. Bui, H. Nguyen, M. M. Tahir, and D. J. Armaghani, (2020) *"Neuro-genetic, neuro-imperialism and genetic programing models in predicting ultimate bearing capacity of pile"* **Engineering with Computers *36***: 1101–1115. DOI: https://doi.org/10.1007/s00366-019-00752-x.

[6] B. R. Murlidhar, R. K. Sinha, E. T. Mohamad, R. Sonkar, and M. Khorami, (2020) *"The effects of particle swarm optimisation and genetic algorithm on ANN results in predicting pile bearing capacity"* **International Journal of Hydromechatronics *3***: 69–87. DOI: https://doi.org/10.1504/IJHM.2020.105484.

[7] T. A. Pham and H.-L. T. Vu, (2021) *"Application of ensemble learning using weight voting protocol in the prediction of pile bearing capacity"* **Mathematical Problems in Engineering *2021***: 5558449. DOI: https://doi.org/10.1155/2021/5558449.

[8] M. Khanmohammadi, D. J. Armaghani, and M. M. S. Sabri, (2022) *"Prediction and optimization of pile bearing capacity considering effects of time"* **Mathematics *10***: 3563. DOI: https://doi.org/10.3390/math10193563.

[9] H. Wang, Z. Lei, X. Zhang, B. Zhou, and J. Peng, (2016) *"Machine learning basics"* **Deep learning**: 98–164.

[10] T. Han, A. Siddique, K. Khayat, J. Huang, and A. Kumar, (2020) *"An ensemble machine learning approach for prediction and optimization of modulus of elasticity of recycled aggregate concrete"* **Construction and Building Materials *244***: 118271. DOI: https://doi.org/10.1016/j.conbuildmat.2020.118271.

[11] M. Bozozuk and M. Bozozuk. *Bearing capacity of pile preloaded by downdrag*. National Research Council Canada, Division of Building Research, 1981.

[12] N. Janbu. "Static bearing capacity of friction piles". In: *Sechste Europaeische Konferenz Fuer Bodenmechanik Und Grundbau*. ***1***. 1976.

[13] M. N. Duc, A. H. Sy, T. N. Ngoc, and T. L. H. Thi. "An artificial intelligence approach based on multi-layer perceptron neural network and random forest for predicting maximum dry density and optimum moisture content of soil material in quang Ninh Province, Vietnam". In: *CIGOS 2021, Emerging Technologies and Applications for Green Infrastructure: Proceedings of the 6th International Conference on Geotechnics, Civil Engineering and Structures*. Springer, 2022, 1745–1754. DOI: https://doi.org/10.1007/978-981-16-7160-9_176.

[14] H. Maizir and K. A. Kassim. "Neural network application in prediction of axial bearing capacity of driven piles". In: *Proceedings of the international multi-conference of engineers and computer scientists*. ***1***. 2013, 13–15. DOI: 10.13140/RG.2.1.4015.0566.

[15] K. Paik and R. Salgado, (2003) *"Determination of bearing capacity of open-ended piles in sand"* **Journal of Geotechnical and Geoenvironmental Engineering *129***: 46–57. DOI: https://doi.org/10.1061/(ASCE)1090-0241(2003)129:1(46).

[16] B. Naeim, M. R. Akbarzadeh, and V. Jahangiri. "Machine learning-based prediction of seismic response of elevated steel tanks". In: *Structures*. ***70***. Elsevier, 2024, 107649. DOI: https://doi.org/10.1016/j.istruc.2024.107649.

[17] L. Wang, Q. Cao, Z. Zhang, S. Mirjalili, and W. Zhao, (2022) *"Artificial rabbits optimization: A new bio-inspired meta-heuristic algorithm for solving engineering optimization problems"* **Engineering Applications of Artificial Intelligence *114***: 105082. DOI: https://doi.org/10.1016/j.engappai.2022.105082.

[18] H. H. Elmousalami, (2020) *"Artificial intelligence and parametric construction cost estimate modeling: State-of-the-art review"* **Journal of Construction Engineering and Management *146***: 03119008. DOI: https://doi.org/10.1061/(ASCE)CO.1943-7862.0001678.

[19] R. S. Benemaran, M. Esmaeili-Falak, and H. Katebi, (2022) *"Physical and numerical modelling of pile-stabilised saturated layered slopes"* **Proceedings of the Institution of Civil Engineers-Geotechnical Engineering *175***: 523–538. DOI: https://doi.org/10.1680/jgeen.20.00152.

[20] W. Gu, J. Liao, and S. Cheng, (2024) *"Bearing capacity prediction of the concrete pile using tunned ANFIS system"* **Journal of Engineering and Applied Science *71***: 39. DOI: https://doi.org/10.1186/s44147-024-00369-y.

[21] N. Chen, (2023) *"Optimizing Pile Bearing Capacity Prediction Using Specific Random Forest Models optimized by Meta-Heuristic Algorithms for Enhanced Geomechanically Applications"* **Advances in Engineering and Intelligence Systems *2***: 101–113. DOI: 10.22034/aeis.2023.426583.1145.

[22] N. Kardani, A. Zhou, M. Nazem, and S.-L. Shen, (2020) *"Estimation of bearing capacity of piles in cohesionless soil using optimised machine learning approaches"* **Geotechnical and Geological Engineering *38***: 2271–2291. DOI: https://doi.org/10.1007/s10706-019-01085-8.

[23] G. G. Meyerhof, (1976) *"Bearing capacity and settlement of pile foundations"* **Journal of the Geotechnical Engineering Division *102***: 197–228. DOI: https://doi.org/10.1061/AJGEB6.0000243.

[24] E. Momeni, H. Maizir, N. Gofar, and R. Nazir, (2013) *"Comparative study on prediction of axial bearing capacity of driven piles in granular materials"* **Jurnal Teknologi *61***: DOI: https://doi.org/10.11113/jt.v61.1777.

[25] E. Avci, (2008) *"Comparison of wavelet families for texture classification by using wavelet packet entropy adaptive network based fuzzy inference system"* **Applied Soft Computing *8***: 225–231. DOI: https://doi.org/10.1016/j.asoc.2007.01.003.

[26] M. Buragohain and C. Mahanta, (2008) *"A novel approach for ANFIS modelling based on full factorial design"* **Applied soft computing *8***: 609–625. DOI: https://doi.org/10.1016/j.asoc.2007.03.010.

[27] A. Sengur, (2008) *"Wavelet transform and adaptive neuro-fuzzy inference system for color texture classification"* **Expert Systems with Applications *34***: 2120–2128. DOI: https://doi.org/10.1016/j.eswa.2007.02.032.

[28] A. Sengur, (2008) *"An expert system based on principal component analysis, artificial immune system and fuzzy k-NN for diagnosis of valvular heart diseases"* **Computers in biology and medicine *38***: 329–338. DOI: https://doi.org/10.1016/j.compbiomed.2007.11.004.

[29] A. J. Riad, H. M. Hasanien, R. A. Turky, and A. H. Yakout, (2023) *"Identifying the PEM fuel cell parameters using artificial rabbits optimization algorithm"* **Sustainability *15***: 4625. DOI: https://doi.org/10.3390/su15054625.

[30] S. Talatahari, M. Azizi, M. Tolouei, B. Talatahari, and P. Sareh, (2021) *"Crystal structure algorithm (CryStAl): a metaheuristic optimization method"* **IEEE Access *9***: 71244–71261. DOI: 10.1109/ACCESS.2021.3079161.

[31] S. A. Farooqui, M. M. Shees, M. F. Alsharekh, S. Alyahya, R. A. Khan, A. Sarwar, M. Islam, and S. Khan, (2021) *"Crystal structure algorithm (CryStAl) based selective harmonic elimination modulation in a cascaded H-bridge multilevel inverter"* **Electronics *10***: 3070. DOI: https://doi.org/10.3390/electronics10243070.

[32] J. C. Thomas, A. R. Natarajan, and A. V. der Ven, (2021) *"Comparing crystal structures with symmetry and geometry"* **npj Computational Materials *7***: 164. DOI: https://doi.org/10.1038/s41524-021-00627-0.